A Research on the Optimization of Certain Plasma Spraying Parameters to Enhance the Shear Adhesion Strength of WC-Ni Coatings on FC300 Material Surfaces

Dang Xuan Thao
Vietnam - Japan Center, Hanoi University of Industry, Hanoi City, Vietnam
dangxuanthao@haui.edu.vn (corresponding author)

Chu Anh Tuan
Vietnam - Japan Center, Hanoi University of Industry, Hanoi City, Vietnam
tuanca1983@gmail.com

Pham Duc Cuong
HaUI Institute of Technology, Hanoi University of Industry, Hanoi City, Vietnam
phamcuong@haui.edu.vn

Received: 23 March 2025 | Revised: 5 May 2025 | Accepted: 8 May 2025

 DOI: https://doi.org/10.48084/etasr.11101

ABSTRACT

Metal-ceramic coatings applied via plasma spraying offer a promising solution for improving the operational durability of machine components. However, the quality of the coating on the surfaces of these components depends on various factors. Among these, the adhesion of the coating plays a crucial role in the lifespan of the component when subjected to relative sliding friction. In addition to material properties, the spraying process parameters have a substantial impact on the coating's adhesion to the substrate metal. This research presents the results of optimizing three spraying parameters: spray current intensity (I_s), powder feed rate (m_s), and spray distance (L_s), concerning the sliding shear adhesion strength (τ_{Sa}) of the metal-ceramic coating with a composition of 34% WC and 45% Ni (WC-45Ni) deposited on the surface of gray cast iron FC300. The coatings were applied using the Atmospheric Plasma Spraying (APS) technique, with particles impacting the substrate surface perpendicularly at a 90° angle. The shear adhesion strength of the coating was determined using a universal compression testing machine (BESTUTM 500HH, Korea). The results indicated that all three input parameters significantly affect the output parameter, with spraying current intensity being the most influential, followed by spraying distance, and powder feed rate recorded as the least influential factor. The optimized spraying parameters, determined through Analysis of Variance (ANOVA), were I_s = 682.3 A, m_s = 31.5 g/min, and L_s = 170.2 mm, resulting in a practical sliding shear adhesion strength of τ_{Sa}= 51.64 MPa. Furthermore, the experimental results were validated with an error of approximately 0.9% compared to the predicted optimal value.

Keywords-shear adhesion strength; WC-Ni coating; plasma spraying; gray cast iron FC300

I. INTRODUCTION

Gray cast iron FC300 is widely utilized in industrial applications, such as machinery manufacturing, cement production, and mining due to its excellent resistance to wear, erosion, corrosion, and vibration. Nonetheless, over prolonged operation, such machine components are subjected to accelerated degradation caused by mechanical loading, friction, thermal exposure, and impact from abrasive particles, which can lead to significant unanticipated operational losses. To mitigate such damage and extend the service life of these components, protective surface coatings are essential.

Among the promising solutions, metal-ceramic coatings based on tungsten carbide (WC) have attracted great attention due to their superior hardness and chemical stability under severe operating conditions. These coatings are typically applied deploying thermal spraying techniques, such as High-Velocity Oxygen Fuel (HVOF) and plasma spraying, which are preferred for their ability to effectively deposit high-melting-point materials. The WC-Ni powder coating, often referred to

as "metal-ceramic", is a multiphase composite where hard ceramic phases are evenly distributed within a ductile metal matrix, providing a balanced combination of hardness and toughness, effectively addressing wear, erosion, and corrosion issues [1-4].

The mechanisms of erosion and wear, as well as the performance of various materials under such conditions have been extensively investigated. WC coatings, along with specific material combinations, have become indispensable in a wide range of industrial, aerospace, and military applications [3, 5]. As a result, several WC coatings on different steel surfaces have been created, showing that protective coatings improve resistance to erosion, corrosion, and wear compared to the inherent performance of the substrate material. It has been indicated that the main factors contributing to the degradation of WC coatings include the gradual removal of the metallic binder, which leads to the disintegration of carbide particle bonding [6-8].

Authors in [9] examined the corrosion resistance of WC-12Co coatings on steel, noting that the Electrochemical Impedance Spectroscopy (EIS) of coated specimens exhibited a larger radius than the bare substrate, indicative of improved corrosion resistance. Similarly, authors in [10] investigated fine WC-NiCr coatings applied via HVOF and optimized spray parameters to prevent excessive heating and carbon loss, thereby minimizing cracking. Authors in [11] studied the influence of Co and Cr content in WC-Co-Cr coatings, revealing that all compositions contained primary and secondary WC phases, along with an amorphous W-Co-Cr phase. Their results showed that the WC-7Co-7Cr coating had the highest hardness and wear resistance, whereas WC-10Co-4Cr exhibited superior corrosion resistance. Authors in [12] investigated the wear and corrosion behavior of WC-based coatings and demonstrated that material degradation under various environmental conditions, such as mechanical wear and corrosive exposure, is primarily governed by mechanisms including grooving, cracking, and pitting, which ultimately lead to material separation. The formation of grooves and pits facilitates the initiation and propagation of cracks within the coating, resulting in the detachment of the softer metallic matrix and the subsequent fragmentation of weakened WC particles. This loss of particle cohesion is a dominant failure mechanism, particularly under sliding wear conditions. In corrosive environments, the degradation process is further exacerbated by plastic deformation and the formation of subsurface cracks, both of which contribute to the progressive removal of material.

Thermal spraying is an effective technique for depositing coatings, such as metal-ceramic materials, owing to its capacity to generate the high energy density and thermal flux required for the complete melting of refractory powders such as WC. Achieving optimal coating properties, such as low porosity and high adhesion strength, depends on multiple factors, including surface pre-treatment, powder composition, and the spraying process parameters. Among these, spray current intensity, powder feed rate, and spray distance have been identified as key variables influencing coating quality [13-15].

In this context, this study focuses on optimizing the APS parameters for WC-45Ni coatings applied to gray cast iron FC300. A Central Composite Design (CCD) with 20 experimental runs was employed in conjunction with ANOVA to identify the optimal spraying conditions. The statistical analysis and modeling were performed using Minitab 19™ software. The optimized parameters were validated experimentally, showing a minimal deviation between predicted and actual values, thus confirming the robustness and predictive reliability of the proposed methodology.

II. EXPERIMENTAL PROCESS AND EVALUATION METHOD

A. Coating Material

1) Coating Sample

Gray cast iron FC300 was selected as the base metal substrate, featuring a chemical composition comprising 3.5% C, 3.0% Si, 0.6% Mn, 0.1% P, 0.12% S, and the rest Fe. To facilitate the plasma spraying process, specimens were manufactured with dimensions of 50 × 40 × 10 mm, as illustrated in Figure 1(a). Prior to coating, the surface of each sample was cleaned and roughened using a shot blasting machine, achieving a surface roughness of approximately Rz ≈ 71 μm (Figure 1(b)) [16]. The WC-45Ni coating was then deposited onto the prepared surface using the APS technique, as depicted in Figure 1(c). Following the coating process, the specimens were sectioned into smaller test samples using an Electrical Discharge Machining (EDM) wire-cutting machine in accordance with the JIS H 8664 standard (Figure 1(d)).

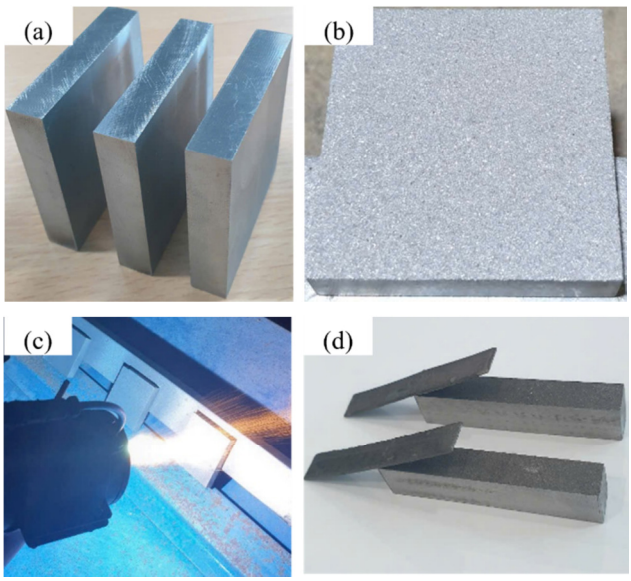

Fig. 1. (a) Post-manufacturing sample, (b) surface-roughened sample, (c) APS coating, (d) cut standard test samples.

2) Coating Powder

WC-Ni powder (Höganäs, Belgium) was utilized in this study. The WC-Ni particles exhibit a size range between 20 μm

and 106 µm, as shown in Figure 2. The chemical composition of the powder is: C ≤ 2.1%, Cr ≤ 10.05%, Ni ≤ 45.05%, Si ≤ 3.25%, Fe ≤ 3.05%, B ≤ 2.25%, and the remainder comprising WC.

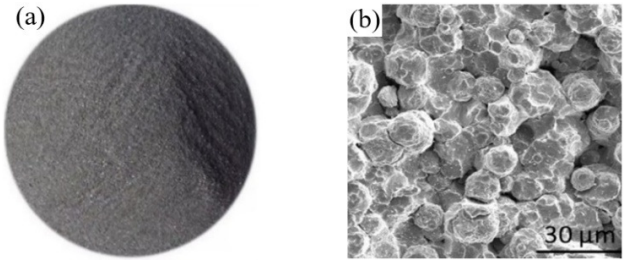

Fig. 2. (a) Image of WC-Ni coating powder, (b) structure of WC-Ni powder.

B. Plasma Coating Process

The spraying process was conducted using a plasma spraying system (Model 3710, PRAXAIR-TAFA, USA) equipped with an SG-100 spray gun. The resulting coating thickness after the spraying process was approximately 1 mm, with a tolerance of +0.2 mm. In this study, the experiments are designed according to the CCD method with 2^k factorial experiments (coded as -1 and +1), 6 central points (coded as 0), and 2k axial points (placed at $-\alpha$ and $+\alpha$, where $\alpha = \sqrt[4]{2^3} = 1.682$) [15]. The values of each input at all levels are shown in Table I.

TABLE I. LEVELS OF PARAMETERS

Parameters	Symbols (unit)	Levels				
		$-\alpha$	*-1*	*0*	*1*	$+\alpha$
Current intensity	I_s (A)	481.82	550	650	750	818.18
Powder feed rate	m_s (g/min)	13.18	20	30	40	46.82
Stand-off distance	L_s (mm)	92.73	120	160	200	227.27

C. Evaluation Method

The samples were evaluated based on the schematic diagram presented in Figure 3.

The τ_{Sa} was determined using a tensile-compression testing machine (Model BESTUTM 500HH, Korea). The results were calculated using:

$$\tau_{Sa} = \frac{P_c}{F} \text{ (MPa)} \quad (1)$$

where: τ_{Sa} is the shear adhesion strength (MPa/mm^2); P_c is the compression force that detaches the coating from the substrate material (N); and F is the cross-section area of the coating (mm^2), which for this study: F = 350 mm^2.

The compressive force required to detach the coating for each sample was recorded and graphically represented by the testing machine, as displayed in Figure 4.

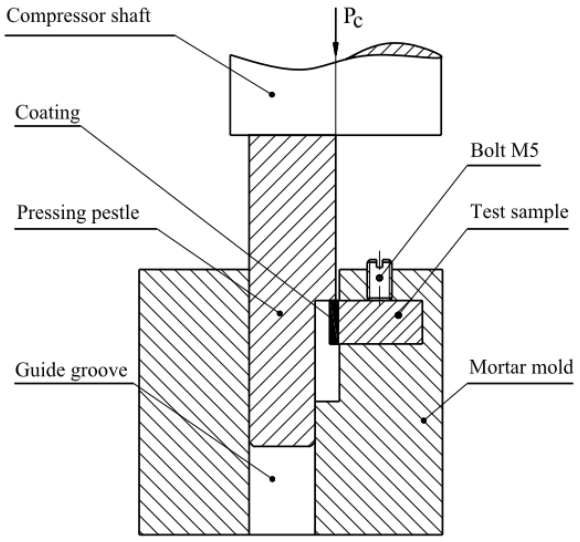

Fig. 3. Schematic diagram of coating adhesion test.

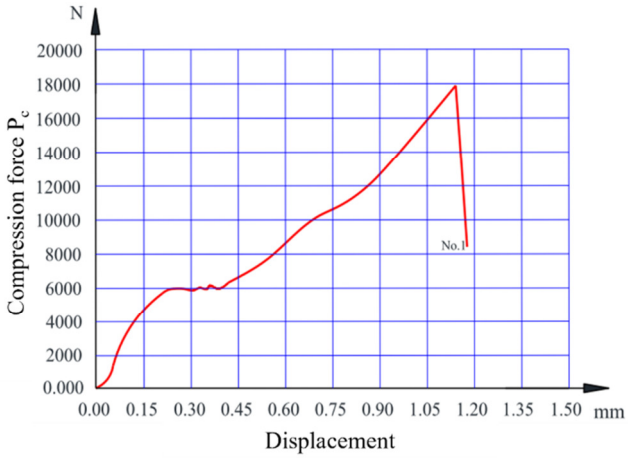

Fig. 4. Characteristic curve of shear adhesion strength.

The analysis of Figure 4 reveals that the characteristic curve is divided into three stages:

- Initial Stage: The applied force increases sharply, reaching approximately 6,000 N within a short displacement range. This stage is attributed to the elastic deformation of the coating layer.
- Second Stage: The graph transitions to a nearly horizontal plateau, indicating that the coating undergoes both plastic and elastic deformation. In this stage, the range is notably short, suggesting that the sprayed coating achieves good quality in terms of hardness and low porosity.
- Third Stage: The force rises steeply again, reaching a peak around 18,000 N after which it rapidly declines. This stage corresponds to the delamination of the coating from the substrate, signifying structural failure and the end of the test.

These observations confirm that the WC–45Ni coating applied by plasma spraying exhibits a typical stress-strain

behavior, with mechanical integrity suitable for practical applications. For each combination of spray parameters, a minimum of three samples were tested, with each measurement conducted on three independent specimens. The average values are reported in Table II. Any data points where the deviation among the three measurements exceeded 5% were excluded from the analysis to ensure reliability and accuracy.

TABLE II. EXPERIMENT MATRIX AND RESULTS

No.	Parameters			Results
	I_s (A)	m_s (g/min)	L_s (mm)	τ_{Sa} (MPa)
1	650	30	160	50.7
2	750	40	120	41.7
3	818.18	30	160	41.1
4	750	20	120	34.4
5	550	40	120	36.1
6	650	30	160	50.9
7	550	20	120	30.1
8	750	20	200	43.4
9	650	30	227.27	40.2
10	650	30	160	52.1
11	650	30	92.73	33.6
12	650	30	160	50.8
13	650	30	160	52.0
14	650	30	160	51.6
15	650	13.18	160	35.7
16	550	40	200	37.2
17	550	20	200	38.2
18	650	46.82	160	39.9
19	750	40	200	45.3
20	481.82	30	160	32.4

D. Experimental Conditions

Besides the three spraying parameters I_s, m_s, and L_s, which are detailed in Table II, the remaining parameters were held constant, including a power supply voltage of 35 V, a plasma gas argon (Ar) flow rate $P_{Ar} = 50$ L/min, a hydrogen (H_2) flow rate $P_{H_2} = 5$ L/min, and an injection angle of 90°.

III. RESULTS AND DISCUSSION

A. Contribution of Parameters on Shear Adhesion Strength

The results of the ANOVA for the influence of the spray parameters (I_s, m_s, L_s), as well as their interaction terms (I_s*m_s, I_s*L_s, m_s*L_s) and polynomial terms (I_s*I_s, m_s*m_s, L_s*L_s) on the shear adhesion strength τ_{Sa} are presented in Table III.

The data in Table III indicate that the P-values associated with the first-order parameters are significantly lower than the selected significance level ($\alpha = 0.05$), confirming that all three spraying parameters (I_s, m_s, L_s) have a statistically significant effect on the τ_{Sa} of the coating. Among these parameters, I_s has the greatest influence on the objective function, accounting for 10.26% of the total 21.26% contribution, followed by L_s (7.76%) and m_s (3.24%). These effects are visualized in Figure 5, where the differences in height between the initial and final points of the response curves for each parameter underscore the varying degrees of impact.

TABLE III. RESULTS OF ANOVA ON SHEAR ADHESION STRENGTH OF THE COATINGS

Source	Degree Freedom (DF)	Sum squared deviation (Seq SS)	Contribution to the model	Average squared (Adj MS)	F-Value	P-Value
Model	9	1003.27	98.20%	111.474	60.66	0.000
Linear	3	217.16	21.26%	72.388	39.39	0.000
I_s	1	104.80	10.26%	104.799	57.03	0.000
m_s	1	33.11	3.24%	33.106	18.02	0.002
L_s	1	79.26	7.76%	79.257	43.13	0.000
Polynomial	3	763.23	74.71%	254.411	138.44	0.000
I_s*I_s	1	225.49	22.07%	323.459	176.02	0.000
m_s*m_s	1	221.49	21.68%	274.741	149.51	0.000
L_s*L_s	1	316.26	30.96%	316.262	172.10	0.000
Interaction	3	22.87	2.24%	7.623	4.15	0.038
I_s*m_s	1	2.21	0.22%	2.205	1.20	0.299
I_s*L_s	1	1.44	0.14%	1.445	0.79	0.396
m_s*L_s	1	19.22	1.88%	19.220	10.46	0.009
Error	10	18.38	1.80%	1.838		
Lack-of-Fit	5	16.40	1.61%	3.280	8.30	0.018
Coefficient of determination R^2: 98.20%						
Adjusted coefficient of determination ($Radj^2$): 96.58%						

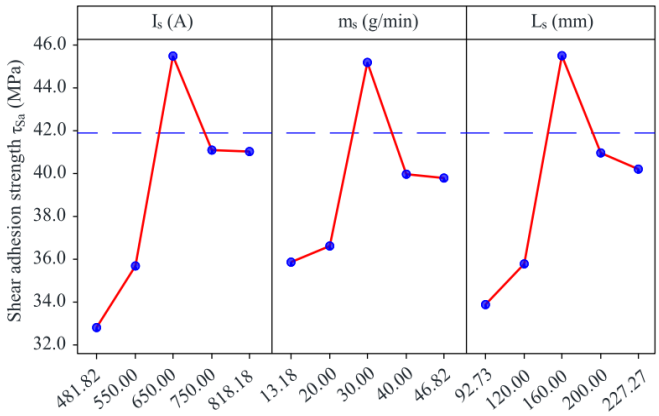

Fig. 5. Influence of parameters on shear adhesion strength.

Meanwhile, based on the analysis of the polynomial term influence shown in Table III, their contribution to τ_{Sa} is 74.71%, with extremely low (~ 0.0001) P-values. This suggests that the inclusion of second-order terms significantly improves the model's explanatory power. Furthermore, the Lack-of-Fit test yields a P-value near 0.0001, indicating that the model's functional form is a good fit for the experimental data. The coefficient of determination (R^2) of the regression function is 98.20%, suggesting a very high degree of correlation between the predicted and observed values.

To further assess the interactions between the parameters, an interaction matrix diagram is provided in Figure 6. This diagram illustrates the complex relationship between pairs of input parameters and their combined effect on the shear adhesion strength.

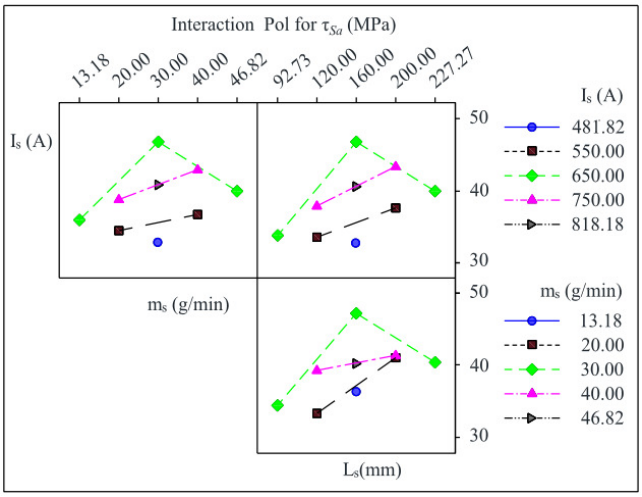

Fig. 6. Influence of interaction between parameters on shear adhesion strength.

A detailed examination of each interaction pair reveals the following:

- At I_s of 650 A, the τ_{Sa} of the coating increases as m_s rises from 13.18 to 30 g/min. However, when m_s continues to increase beyond 30 g/min to 46.82 g/min, the τ_{Sa} declines. For I_s values of 550 A and 750 A, increasing ms from 20 to 40 g/min results in enhanced τ_{Sa}, with a more pronounced effect observed at 750 A. This behavior can be attributed to the higher combustion chamber temperatures associated with elevated I_s levels, which enhance the melting of spray particles and improve cohesion. Conversely, as m_s increases, the larger quantity of particles entering the spraying zone may hinder uniform melting due to heat dissipation, reducing inter-particle bonding and ultimately decreasing τ_{Sa}.
- Interaction between I_s and L_s: For an I_s of 650 A, increasing L_s from 92.73 mm to 160 mm enhances τ_{Sa}. However, beyond 160 mm to 227.2 mm, τ_{Sa} begins to decline. This trend is consistent for I_s values of 550 A and 750 A, with τ_{Sa} improving as L_s increases from 120 mm to 200 mm. The effect of L_s is more significant at 750A. This can be explained by particle dynamics, where increasing L_s leads to re-solidification of the particles due to cooling, and the smaller the particles are, the faster is the re-solidification. At the same time, more oxidized particles cause the reduction of the coating cohesion and τ_{Sa} [17]. On the other hand, lowering L_s limits the spraying effectiveness owing to the strong impact force with the steel, causing the particles to be thrown out.
- Interaction between m_s and L_s: At a constant m_s of 30 g/min, increasing L_s from 92.73 mm to 160 mm improves τ_{Sa}, but a further increase beyond 160 mm up to 227.27 mm results in degradation. For m_s values between 20 and 40 g/min, increasing L_s within the range of 120 mm to 200 mm consistently enhances τ_{Sa}, with a greater effect observed at 40 g/min. This can be explained by the fact that an increase in L_s leads to a reduction in the kinetic energy of the particles, which in turn lowers the coating's cohesion [17]. At lower m_s levels, the τ_{Sa} of the coating increases, due to a decrease in the particle density entering the spray chamber, resulting in improved heating efficiency of the spray particles. However, excessively increasing m_s causes a drop in the arc temperature within the combustion chamber, which reduces particle velocity and, as a result, diminishes both the quality and τ_{Sa} of the coating. Hence, reducing L_s becomes essential at higher m_s to maintain coating performance.

B. Regression Model of Shear Adhesion Strength Determination

The empirical equation based on regression analysis showing the relationship between the coating's shear adhesion strength and the spraying parameters is:

$$\tau_{Sa} = -292.7 + 0.6108 \cdot I_s + 3.054 \cdot m_s + 1.044 \cdot L_s - 0.000474 \cdot I_s * I_s - 0.04365 \cdot m_s * m_s - 0.002928 \cdot L_s * L_s + 0.000525 \cdot I_s * m_s + 0.000106 \cdot I_s * L_s - 0.00388 \cdot m_s * L_s \quad (2)$$

The empirical equation (2) has a coefficient of determination $R^2 = 0.98$, indicating strong agreement with the experimental data.

This equation is the basis for selecting the values of the spray parameters (I_s, m_s, and L_s) to ensure that the coating's shear adhesion strength reaches a specific suitable value. The comparison results between the predicted and experimental shear adhesion strength are shown in Table IV and Figure 7.

TABLE IV. COMPARISON BETWEEN THE PREDICTED AND EXPERIMENTAL SHEAR ADHESION STRENGTH

No.	Experimental τ_{Sa} (MPa)	Predicted τ_{Sa} (MPa)	Difference (%)
1	50.7	51.1	0.8
2	41.7	40.9	2.0
3	41.1	42.3	2.9
4	34.4	33.6	2.3
5	36.1	35.2	2.5
6	50.9	51.1	0.4
7	30.1	30.1	0.2
8	43.4	42.3	2.5
9	40.2	41.9	4.1
10	52.1	51.1	1.9
11	33.6	33.9	0.8
12	50.8	51.1	0.6
13	52.0	51.1	1.7
14	51.6	51.1	0.9
15	35.7	36.1	1.3
16	37.2	36.0	3.2
17	38.2	37.1	3.0
18	39.9	41.4	3.7
19	45.3	43.4	4.2
20	32.4	33.1	2.2
Average difference			2.1

The results demonstrate close alignment, with a maximum error of 4.2% and an average error of 2.1%. Therefore, the proposed model (2) has been validated and can be effectively used for prediction and optimization.

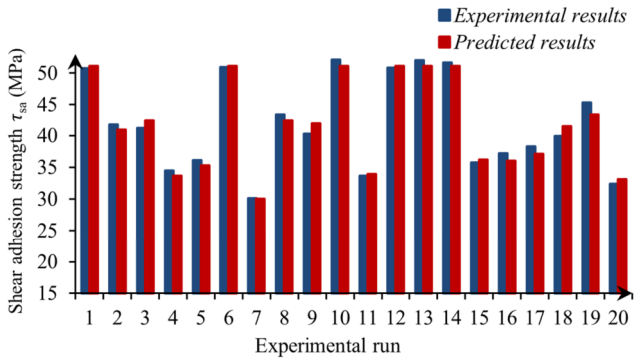

Fig. 7. The predicted and experimental results of shear adhesion strength.

C. Optimization Result for Shear Adhesion Strength

To solve the problem of optimizing the shear adhesion strength of the coating with the highest value in specific conditions, Minitab 19™ software is applied. The obtained optimization results are illustrated in Figure 8.

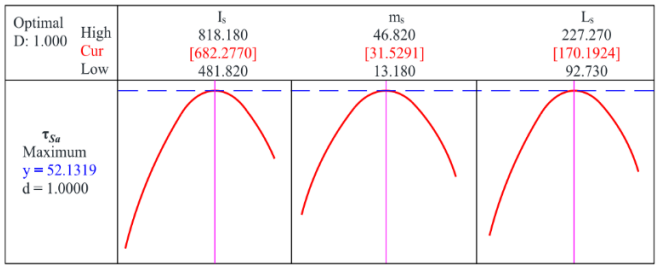

Fig. 8. Graphs showing the relationship between spraying parameters and shear adhesion strength.

Next, a Genetic Algorithm (GA) was employed for optimization using the following parameters: a population size of 100, a crossover probability of 0.25, a mutation probability of 0.05, and a mutation parameter of 4. The optimization results are presented in Figure 9.

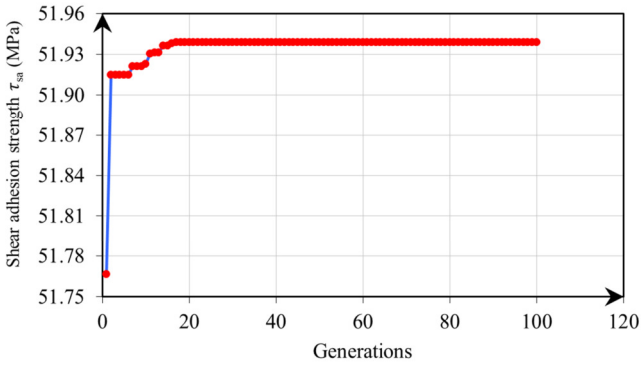

Fig. 9. Optimization results using GA.

Table V compares the solutions obtained using both optimization methods for maximizing the shear adhesion strength of the WC–45Ni coating. The comparison reveals minimal differences in the identified parameters, and that the predicted shear adhesion strength values are nearly identical. Therefore, the derived parameter set can be considered optimal for achieving the desired coating shear adhesion strength.

TABLE V. RESULTS OF THE OPTIMAL SET OF PARAMETERS BY TWO METHODS: ANOVA AND GA

Solution	I_s (A)	m_s (g/min)	L_s (mm)	τ_{Sa} (MPa)
ANOVA	682.3	31.5	170.2	52.1
GA	680.7	31.5	169.7	51.9
Difference (%)	0.23	0.00	0.29	0.38

D. Results for examining the optimization according to ANOVA and GA

To assess the suitability of the optimized spraying parameters from ANOVA and GA, an experiment was conducted to examine 5 specimens. The measurement results of each sample and the average results examined by the two methods are listed in Table VI.

TABLE VI. MEASUREMENT RESULTS ON SAMPLES FOR EXAMINING OPTIMIZATION

Solution	Results by sample (MPa)					Result (MPa)		Diff. (%)
	1	2	3	4	5	Exp.	Pred.	
ANOVA	53.4	51.1	50.5	50.9	52.3	51.64	52.1	0.9
GA	50.2	49.6	53.5	49.8	51.5	50.92	51.9	1.9

Based on the results in Table VI, the experimental values for both methods closely match the calculated results, with errors of 0.9% for the ANOVA-optimized parameters and 1.9% for the GA. This further confirms that the optimized parameters from both methods are suitable for practical application. Since the ANOVA-optimized parameters demonstrate superior performance, the set of parameters I_s = 682.3 A, m_s = 31.5 g/min, and L_s = 170.2 mm is proposed to achieve the maximum shear adhesion strength for plasma spraying WC–45Ni powder onto an FC300 steel substrate in practical settings.

IV. CONCLUSION

This study investigates the deposition of WC–45Ni coatings on FC300 steel using Atmospheric Plasma Spraying (APS). Three key process parameters, plasma current intensity (I_s), powder feed rate (m_s), and stand-off distances (L_s), were examined and optimized via Central Composite Design (CCD) combined with Analysis of Variance (ANOVA) and a Genetic Algorithm (GA), focusing on maximizing the coating's shear adhesion strength (τ_{Sa}). The main findings are:

- Among the parameters studied, I_s has the greatest influence on the shear adhesion strength of the WC-45Ni coating, followed by L_s and m_s.
- Using the GA method, the optimal parameters are I_s = 680.7 A, m_s = 31.5 g/min, L_s = 169.7 mm for the coating, predicting a maximum shear adhesion strength of 51.9 MPa. The experimental testing yielded 50.92 MPa, with a 1.9% prediction error, confirming the effectiveness of these settings for producing high-quality coatings.

- With the ANOVA method, the proposed parameters are I_s = 682.3 A, m_s = 31.5 g/min, L_s = 170.2 mm for the coating, predicting a maximum shear adhesion strength of 52.1 MPa. The measured strength was 51.64 MPa, a 0.9% prediction error, indicating that ANOVA-based optimization provides slightly more stable and reliable parameters than GA.
- Beyond these results, this study presents a novel, systematic optimization approach integrating CCD, ANOVA, and GA to enhance shear adhesion strength of WC–45Ni coatings on gray cast iron (FC300)—a substrate rarely explored in previous research. Moreover, the achieved adhesion strengths (up to 51.64 MPa) underscore the technical significance and practical applicability of the proposed method for developing high-performance coatings in engineering applications.

ACKNOWLEDGMENT

This research is supported by Hanoi University of Industry through the science and technology program. Contract code 06-2023-RD/HD-DHCN.

REFERENCES

[1] S. Seethammaraju and M. Rangarajan, "Corrosion of stainless steels in acidic, neutral and alkaline saline media: Electrochemical and microscopic analysis," *IOP Conference Series: Materials Science and Engineering*, vol. 577, no. 1, Nov. 2019, Art. no. 012188, https://doi.org/10.1088/1757-899X/577/1/012188.

[2] Q. B. Nguyen *et al.*, "The role of abrasive particle size on erosion characteristics of stainless steel," *Engineering Failure Analysis*, vol. 97, pp. 844–853, Mar. 2019, https://doi.org/10.1016/j.engfailanal. 2019.01.020.

[3] P. S. Babu, Y. Madhavi, L. R. Krishna, G. Sivakumar, D. S. Rao, and G. Padmanabham, "Thermal Spray Coatings for Erosion–Corrosion Resistant Applications," *Transactions of the Indian Institute of Metals*, vol. 73, no. 9, pp. 2141–2159, Sep. 2020, https://doi.org/10.1007/s12666-020-02053-0.

[4] A. R. Govande, A. Chandak, B. R. Sunil, and R. Dumpala, "Carbide-based thermal spray coatings: A review on performance characteristics and post-treatment," *International Journal of Refractory Metals and Hard Materials*, vol. 103, Feb. 2022, Art. no. 105772, https://doi.org/10.1016/j.ijrmhm.2021.105772.

[5] Z. Ke *et al.*, "Microstructure and mechanical properties of dual-grain structured WC-Co cemented carbides," *Ceramics International*, vol. 45, no. 17, pp. 21528–21533, Dec. 2019, https://doi.org/10.1016/j.ceramint. 2019.07.146.

[6] A. Koutsomichalis, M. Vardavoulias, and N. Vaxevanidis, "HVOF sprayed WC-CoCr coatings on aluminum: tensile and tribological properties," *IOP Conference Series: Materials Science and Engineering*, vol. 174, Feb. 2017, Art. no. 012062, https://doi.org/10.1088/1757-899X/174/1/012062.

[7] R. J. K. Wood, S. Herd, and M. R. Thakare, "A critical review of the tribocorrosion of cemented and thermal sprayed tungsten carbide," *Tribology International*, vol. 119, pp. 491–509, Mar. 2018, https://doi.org/10.1016/j.triboint.2017.10.006.

[8] S. Hong, Y. Wu, W. Gao, J. Zhang, Y. Zheng, and Y. Zheng, "Slurry erosion-corrosion resistance and microbial corrosion electrochemical characteristics of HVOF sprayed WC-10Co-4Cr coating for offshore hydraulic machinery," *International Journal of Refractory Metals and Hard Materials*, vol. 74, pp. 7–13, Aug. 2018, https://doi.org/10.1016/j.ijrmhm.2018.02.019.

[9] K. Weicheng, S. Hui, G. Jiaxu, W. Jie, and L. Yuling, "Electrochemical corrosion behavior of HVOF sprayed WC–12Co coating on H13 hot work mould steel," *Anti-Corrosion Methods and Materials*, vol. 66, no. 6, pp. 827–834, Nov. 2019, https://doi.org/10.1108/ACMM-12-2018-2051.

[10] S. Singh *et al.*, "Development of fine WC-NiCr powder coatings by optimising HVOF spray parameters," *International Journal of Refractory Metals and Hard Materials*, vol. 121, Jun. 2024, Art. no. 106667, https://doi.org/10.1016/j.ijrmhm.2024.106667.

[11] Q. Wang *et al.*, "Effect of Cobalt and Chromium Content on Microstructure and Properties of WC-Co-Cr Coatings Prepared by High-Velocity Oxy-Fuel Spraying," *Materials*, vol. 16, no. 21, Nov. 2023, Art. no. 7003, https://doi.org/10.3390/ma16217003.

[12] K. Torkashvand, S. Joshi, and M. Gupta, "Advances in Thermally Sprayed WC-Based Wear-Resistant Coatings: Co-free Binders, Processing Routes and Tribological Behavior," *Journal of Thermal Spray Technology*, vol. 31, no. 3, pp. 342–377, Feb. 2022, https://doi.org/10.1007/s11666-022-01358-4.

[13] Y. Wang *et al.*, "Effect of spraying power on the morphology of YSZ splat and micro-structure of thermal barrier coating," *Ceramics International*, vol. 47, no. 13, pp. 18956–18963, Jul. 2021, https://doi.org/10.1016/j.ceramint.2021.03.238.

[14] H. T. Nguyen, T. L. Nguyen, V. T. Nguyen, and L. Hoang, "Investigation of the Impact of HVOF Spraying Parameters on the Abrasion Resistance of Tungsten Carbide Coatings," *Engineering, Technology & Applied Science Research*, vol. 14, no. 6, pp. 17769–17773, Dec. 2024, https://doi.org/10.48084/etasr.7996.

[15] R. C. Tucker, Ed., *Thermal Spray Technology*. ASM International, 2013.

[16] P. D. Cuong and D. X. Thao, "Effect of surface roughness and plasma current to adhesion of Cr3C2-NiCr coating fabricated by plasma spray technique on 16Mn steel," *International Journal of Modern Physics B*, vol. 35, no. 14n16, Jun. 2021, Art. no. 2140037, https://doi.org/ 10.1142/S0217979221400373.

[17] A. Buketov, O. Syzonenko, D. Kruglyj, T. Cherniavska, E. Appazov, and K. Klevtsov, "Investigation of the Influence of the Synthesized Iron-Carbide Mixture on the Adhesive and Mechanical Properties of Epoxy Composites for Parts of Transport Machines," *Engineering, Technology & Applied Science Research*, vol. 10, no. 5, pp. 6214–6219, Oct. 2020, https://doi.org/10.48084/etasr.3750.